Available online at www.sciencedirect.com
SCIENCE DIRECT®
Journal of Solid State Chemistry 174 (2003) 302–309
JOURNAL OF SOLID STATE CHEMISTRY
http://elsevier.com/locate/jssc

Crystal structure and magnetic properties of the UFe_7Al_5 uranium–iron aluminide

A.P. Gonçalves,[a,*] J.C. Waerenborgh,[a] M. Almeida,[a] and H. Noël[b]

[a] *Departamento de Química, Instituto Tecnológico e Nuclear, Estrada Nacional 10, P-2686-953 Sacavém, Portugal*
[b] *Laboratoire de Chimie du Solide et Inorganique Moléculaire. UMR CNRS 6511, Université de Rennes 1, Avenue de Général Leclerc, 35042 Rennes, France*

Received 3 February 2003; received in revised form 8 April 2003; accepted 17 April 2003

Abstract

The ternary compound UFe_7Al_5 was synthesized by arc melting, followed by annealing at 850°C. The crystal structure was determined by single-crystal X-ray diffraction and refined to a residual value of $R = 0.039$ ($S = 1.030$), with lattice parameters $a = 8.581(2)$ Å and $c = 4.946(1)$ Å. This compound is a new extreme composition in the family of intermetallics with general formula UFe_xAl_{12-x} crystallizing in the tetragonal $ThMn_{12}$-type structure, space group *I4/mmm*. In contrast to UFe_xAl_{12-x} within the composition range $4 \leqslant x \leqslant 6$, in UFe_7Al_5 the additional iron atom is found in the 8*i* equipositions. Magnetization measurements versus temperature show two magnetic transitions at 363 and 275 K, respectively, with a ferromagnetic behavior below the highest temperature transition. ^{57}Fe Mössbauer data indicate that the high-temperature transition is related to the ordering of the iron atoms. The dependence of the isomer shifts and magnetic hyperfine fields on the crystallographic site and on the number of the iron nearest neighbors is similar to that observed in the other UFe_xAl_{12-x} and rare-earth analogues. The magnetic hyperfine field values of iron atoms on 8*i* sites is larger than in the other sites, in agreement with previous data obtained for other $ThMn_{12}$-type compounds.

Keywords: UFe_7Al_5; Uranium intermetallic; Magnetic intermetallic; $ThMn_{12}$-type structure

1. Introduction

Compounds of *f*-elements with the $ThMn_{12}$-type structure and high iron content have been considered as good candidates for hard magnetic materials [1,2]. The isostructural AFe_{12} (A = *f*-element) binary compounds do not exist, and to stabilize this type of structure it is necessary to partially substitute the iron by a *d* or *p* element.

One of the earliest investigated compounds with the $ThMn_{12}$-type structure belongs to the series AFe_xAl_{12-x}, with A = *f*-element, first studied on polycrystalline samples with rare earths [3,4], and later with actinides [5,6]. In these systems, it was found that the aluminum concentration necessary to stabilize the $ThMn_{12}$-type structure is relatively high, usually more than 50%. They present complex magnetic properties, even in the simplest cases such as LFe_4Al_8 (L = Y, Lu), where the iron atoms are located in only one crystallographic position (8*f*) and the *f*-element is non-magnetic [7].

Studies on UFe_4Al_8 single crystals showed that the main magnetic interaction is a commensurate antiferromagnetic ordering of the iron sublattice leading to a transition temperature of ~150 K. A weak ferromagnetic component from the iron atoms, due to a small canting of the moments, and a ferromagnetic ordering of the uranium moments were also observed at the same temperature, both contributions parallel to the easy *a* and *b* directions [8,9]. Previous measurements on UFe_5Al_7 and UFe_6Al_6 polycrystalline samples indicated a ferromagnetic character for both compounds [6,10]. In these compounds, powder neutron diffraction results suggested that the iron moments are ferromagnetically ordered in a configuration perpendicular to the *c*-axis [10,11].

The UFe_xAl_{12-x} phase relations, previously explored by our group, indicated a congruent melting composition range between $UFe_{3.8}Al_{8.2}$ and $UFe_{5.8}Al_{6.2}$ [12]. The magnetic phase diagram of this system was

*Corresponding author. Fax: +351-1-9941455.
E-mail address: apg@itn.pt (A.P. Gonçalves).

0022-4596/03/$ - see front matter © 2003 Elsevier Inc. All rights reserved.
doi:10.1016/S0022-4596(03)00224-X

previously determined in this composition range, and four magnetic regions were identified, with two transitions in the range between $x = 4$ and x slightly below 5 [13]. More recently, in the course of a systematic study of the U–Fe–Al ternary phase diagram, we found that it is possible to obtain almost single-phase samples with a higher iron concentration and the $ThMn_{12}$-type structure [14]. Herein, we report on the crystallographic structure determination, from powder and single-crystal X-ray diffraction data, and on the magnetic properties, studied by magnetization and ^{57}Fe Mössbauer spectroscopy measurements, of the new extreme composition of this series, UFe_7Al_5.

2. Experimental

Samples with UFe_7Al_5 nominal composition, each weighing ~ 0.4 g, were prepared by arc-melting ingots of the constituents with purity higher than 99.9%, on a water-cooled copper crucible under Ti-gettered high-purity argon atmosphere. The surface of the uranium ingots was cleaned in diluted HNO_3 prior to use. Repeated melting was used in order to ensure a better homogeneity. The weight losses were less than 0.5 wt.%.

Each button was wrapped in molybdenum foil, sealed in evacuated quartz ampoules and annealed for 360 h at 850°C, followed by rapid cooling to room temperature.

A microstructural analysis of the samples was performed with a SEM/EDS (JEOL-JSM 840) apparatus on polished surfaces. Quantitative analysis of the observed phases was made by EDS analysis of the atomic characteristic X-rays excited by the electron beam operating at 15 kV.

The samples were examined by X-ray powder diffraction using a INEL CPS 120 diffractometer. Silicon powder was added to the material and used as an internal standard. The room-temperature lattice parameters were obtained by least-squares fits using the program UnitCell [15].

A single crystal suitable for X-ray measurements, with approximate dimensions $0.09 \times 0.05 \times 0.03\,mm^3$, was isolated from the polycrystalline material, glued on the top of a glass fiber and mounted on the goniometer head. X-ray single-crystal diffraction data were collected using a four-circle diffractometer Enraf–Nonius CAD-4 with graphite monochromatized Mo$K\alpha$ radiation ($\lambda = 0.71069$ Å). The lattice parameters were obtained by least-squares refinement of the 2θ values of 25 intense and well-centered reflections (from various regions of the reciprocal space in the $19° < 2\theta < 39°$ range).

The data were recorded at room temperature in a $\omega - 2\theta$ scan mode ($\Delta\omega = 0.80 + 0.35 \tan\theta$). Two reflections were monitored as intensity and three as orientation standards at 240 min intervals during data collection; no variation larger than 5% was observed. The intensities of the 5145 measured reflections (with $6° \leqslant 2\theta \leqslant 90°$) were corrected for absorption by an empirical method based on Ψ scans [16], and for Lorentz and polarization effects. The reflections were averaged, resulting in 448 independent reflections, from which 347 were considered significant ($I > 4\sigma(I)$).

The diffraction data are compatible with a tetragonal system, space group *I4/mmm*. The structure was refined employing the program SHELX-97 [17] and assuming a $ThMn_{12}$-type structure [18]. The extinction factor, scale factor, two position parameters (x for the 8*j* and 8*f* crystallographic positions), three occupation factors and 12 anisotropic temperature factors were refined. The iron and aluminum contents in each of the 8*f*, 8*i* and 8*j* positions were allowed to vary with the constraint of full-site occupation. Crystallographic and experimental data of the structural determination are listed in Table 1.

The determination of the Wigner–Seitz cell topology and volume was performed using the DIDO95 software program [20]. This program uses the radical method [21] for constructing the Wigner–Seitz cells. In this method, the perpendicular bisecting planes are located in proportion to the assigned atomic radii of the atoms,

Table 1
Crystallographic and experimental data of the UFe_7Al_5 X-ray single-crystal measurement

Chemical formula	UFe_7Al_5
Formula weight	763.9 g/mol
Crystal system	Tetragonal
Space group [19]	*I4/mmm* (No. 139)
a	8.581(2) Å
c	4.946(1) Å
V	364.2(1) Å^3
Z	2
D_{calc}	6.97 g cm^{-1}
μ(Mo$K\alpha$) (cm^2 g^{-1})	36.18
Approximate crystal dimensions $0.09 \times 0.05 \times 0.03$ mm^3	
Radiation, wavelength	Mo$K\alpha$, 0.71073 Å
Monochromator	Graphite
Temperature	295 K
θ range	3–45°
ω–2θ scan	$\Delta\omega = 0.80 + 0.35 \tan\theta$
Data set	$-10 \leqslant h \leqslant 15$, $-15 \leqslant k \leqslant 15$, $-9 \leqslant l \leqslant 9$
Crystal-to-receiving-aperture distance	173 mm
Horizontal, vertical aperture	4.4 mm
Total data	5145
Unique data	448
Observed data ($I \geqslant 4\sigma(I)$)	347
Number of refined parameters	22
Final agreement factors[a]	
$R = \sum\|F_{obs} - F_{calc}\| / \sum\|F_{obs}\|$	0.039
$wR = \left[\sum\left(w(\|F_{obs}\| - \|F_{calc}\|)^2\right) / \sum w\|F_{obs}\|^2\right]^{1/2}$	0.111
$S = \left[\sum w(\|F_{obs}\| - \|F_{calc}\|)^2 / (m-n)\right]^{1/2}$	1.030

leading to a more realistic calculation of the Wigner–Seitz cell volume.

Magnetization measurements were performed on the polycrystalline samples after zero field cooling (ZFC) and field cooling (FC). The measurements were carried out in the 5–400 K temperature range and under fields up to 8 T by an extraction technique using a Maglab2000 system (Oxford Instruments).

Part of the sample was powdered and pressed together with lucite powder into a perspex holder in order to obtain a homogeneous and isotropic Mössbauer absorber containing $\approx 5\,mg/cm^2$ of natural iron. ^{57}Fe Mössbauer measurements were performed in transmission mode using a conventional constant acceleration spectrometer and a 25 mCi ^{57}Co source in Rh matrix. The velocity scale was calibrated using an α-Fe foil at room temperature. Spectra were collected between 296 and 5 K. Low-temperature spectra were obtained using a flow cryostat (temperature stability ± 0.5 K).

The spectra were fitted to lorentzian lines using a non-linear least-squares fitting method [22]. More than one sextet was fitted to the corresponding spectra; the widths ($\Gamma_{1,6}, \Gamma_{2,5}, \Gamma_{3,4}$) and the relative areas ($I_{1,6}, I_{2,5}, I_{3,4}$) of peaks (1–6), (2–5) and (3–4) in each magnetic splitting were always kept equal during refinement. The ratio of the relative areas $I_{1,6}/I_{2,5}/I_{3,4}$ were kept equal to 3:2:1 for each sextet but the linewidths of each line pair were allowed to vary and were found to slightly increase from the inner to the outer lines of each sextet, typically $\Gamma_{1,6}/\Gamma_{2,5}/\Gamma_{3,4} \approx 1.2/1.1/1.0$. Further constraints were used as explained in the next section.

3. Results and discussion

The EDS elemental analysis of the sample confirmed that the main phase composition is $U_{1.0(1)}Fe_{6.99(4)}Al_{5.01(4)}$, very close to the nominal U:7Fe:5Al ratio of the elements. However, a minority phase, with 66 at.% iron and 34 at.% aluminum composition, could be also detected.

Almost all the peaks of the X-ray powder diffractograms could be indexed according to the tetragonal structure. Only a small extra peak could be detected, corresponding to a 2.052 Å interatomic distance, confirming the presence of FeAl-type phases (with the most intense peak reported at ~ 2.056 Å [23]), but with a concentration lower than 1 wt.%. The Fe–Al binary phase diagram indicates that at this annealing temperature, the atomic percentage of aluminum in the FeAl-type phases can vary between 25 and 51 at.%, in agreement with the 34 at.% aluminum composition found by EDS.

The refinement of the lattice parameters using the 26 most intense reflections of the powder pattern in the range $10° \leqslant 2\theta \leqslant 100°$, down to a residual $R(2\theta) = 0.023$, gives the tetragonal lattice parameters $a = 8.594(1)$ Å and $c = 4.952(1)$ Å, and a cell volume of $365.8(1)$ Å^3. The refinement of the lattice parameters using X-ray single-crystal diffraction data yields values similar to those obtained from the powder measurements ($a = 8.581(2)$ Å and $c = 4.946(1)$ Å). The least-squares procedure for refinement of occupation factors, positional and anisotropic thermal parameters for all atoms converged to $R = 0.039$ and $S = 1.030$, confirming for UFe_7Al_5 the $ThMn_{12}$-type structure. The refined occupation factors, atomic positions and anisotropic thermal parameters are presented in Table 2.

The unit cell of UFe_7Al_5 is illustrated in Fig. 1. The present refinement shows that the uranium atoms are located on the 2*a* site, and the iron atoms fully occupy the 8*f*, approximately half of the 8*j* and one-fourth of

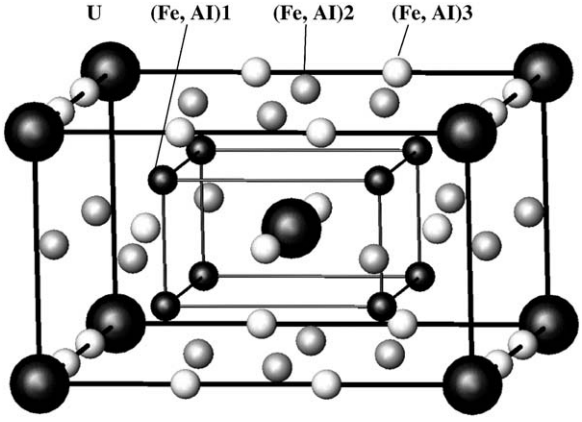

Fig. 1. Unit cell of UFe_7Al_5.

Table 2
Positional parameters (x, y, z), occupation factors (OFs), anisotropic temperature factors (U_{kl}), and their estimated standard deviations

Atom	Position	x	y	z	OF	U_{11} (Å^2)	U_{22} (Å^2)	U_{33} (Å^2)	U_{23} (Å^2)	U_{13} (Å^2)	U_{12} (Å^2)	U_{eq} (Å^2)
U	2*a*	0	0	0	1	0.0111(3)	0.0111(3)	0.0128(3)	0	0	0	0.0117(2)
Fe	8*f*	1/4	1/4	1/4	0.97(3)	0.0063(5)	0.0063(5)	0.0056(6)	0.0007(2)	0.0007(2)	0.0001(3)	0.0060(4)
Al	8*f*	1/4	1/4	1/4	0.03(3)	0.0063(5)	0.0063(5)	0.0056(6)	0.0007(2)	0.0007(2)	0.0001(3)	0.0060(4)
Fe	8*j*	0.2766(3)	1/2	0	0.49(3)	0.014(1)	0.0045(9)	0.0064(8)	0	0	0	0.0082(6)
Al	8*j*	0.2766(3)	1/2	0	0.51(3)	0.014(1)	0.0045(9)	0.0064(8)	0	0	0	0.0082(6)
Fe	8*i*	0.3474(4)	0	0	0.22(3)	0.011(1)	0.007(1)	0.011(1)	0	0	0	0.0096(8)
Al	8*i*	0.3474(4)	0	0	0.78(3)	0.011(1)	0.007(1)	0.011(1)	0	0	0	0.0096(8)

Table 3
UFe_7Al_5 interatomic distances (d) and nearest neighbors (NNs) average numbers

	NN	Atoms	d (Å)		NN	Atoms	d (Å)
U (2*a*)	8	(Fe,Al)1 (8*f*)	3.276(1)	(Fe,Al)1 (8*f*)	2	(Fe,Al)1 (8*f*)	2.4730(5)
	8	(Fe,Al)2 (8*j*)	3.129(2)		4	(Fe,Al)2 (8*j*)	2.487(1)
	4	(Fe,Al)3 (8*i*)	2.981(3)		4	(Fe,Al)3 (8*i*)	2.613(1)
					2	U (2*a*)	3.276(1)
(Fe,Al)2 (8*j*)	4	(Fe,Al)1 (8*f*)	2.487(1)	(Fe,Al)3 (8*i*)	4	(Fe,Al)1 (8*f*)	2.613(1)
	2	(Fe,Al)2 (8*j*)	2.711(4)		2	(Fe,Al)2 (8*j*)	2.692(2)
	2	(Fe,Al)3 (8*i*)	2.692(2)		2	(Fe,Al)2 (8*j*)	2.711(3)
	2	(Fe,Al)3 (8*i*)	2.711(3)		1	(Fe,Al)3 (8*i*)	2.620(6)
	2	U (2*a*)	3.129(2)		4	(Fe,Al)3 (8*i*)	3.090(3)
					1	U (2*a*)	2.981(3)

the 8*i* sites, the remaining being occupied by aluminum. The significant 8*i* site iron occupation factor is somehow surprising, as all the previous studies in UFe_xAl_{12-x} and rare-earth RFe_xAl_{12-x} ($4<x<6$) compounds indicated that this element largely avoids the 8*i* site [22,24]. An important iron concentration in the 8*i* site was previously observed in $UFe_7Al_3Si_2$ samples [25], but the presence of silicon, which goes to the 8*f* and 8*j* sites [26], could be the reason for this abnormal distribution. The final refined composition converges to $UFe_{6.7(4)}Al_{5.3(4)}$, in good agreement with the nominal composition.

The number of nearest neighbors and interatomic distances (up to 3.30 Å), obtained in the X-ray refinement for the different crystallographic positions, are listed in Table 3.

The uranium-nearest-neighbor interatomic distances are usually larger than the sum of the uranium and the weighed metallic radii, 2.79, 2.88 and 2.92 Å for 8*f*, 8*j* and 8*i* crystallographic positions, respectively (the correspondent weighed metallic radii, 1.26, 1.35 and 1.39 Å for 8*f*, 8*j* and 8*i* positions, were calculated considering the refined occupation factors and an atomic radii of 1.26 Å for iron, 1.43 Å for aluminum and 1.53 Å for uranium, for a coordination number of 12 [27]). The higher uranium coordination number of 20, when compared with the coordination number of 12 of the given metallic radii, can partially explain the observed long distances. The only exception is the 8*i* position, which is at 2.981 Å, a value close to the sum of the metallic radii (2.92 Å). No other uranium atoms are on the U nearest coordination sphere.

All the interatomic distances between (Fe,Al)1 (8*f*) and the nearest iron positions are below the metallic radii sum, 2.52, 2.61 and 2.65 Å for 8*f*, 8*j* and 8*i*, respectively. The (Fe,Al)2 (8*j*) atoms also have most of the next neighbors at distances below the sum of the metallic radii (2.61, 2.70 and 2.74 Å for 8*f*, 8*j* and 8*i*, respectively), the only exceptions being the two (Fe,Al)2 next neighbors close to that value. In the case of (Fe,Al)3 (8*i*), and due to its higher coordination number, a slight increase of the interatomic distances could be expected. Indeed, albeit most of the iron positions are at distances below the metallic radii sum, four of the (Fe,Al)3 (8*i*) atoms are at distances larger (3.090 Å) and two of the (Fe,Al)2 (8*j*) are close (2.711 Å) to that sum (2.78 and 2.74 Å for 8*i* and 8*j* positions, respectively).

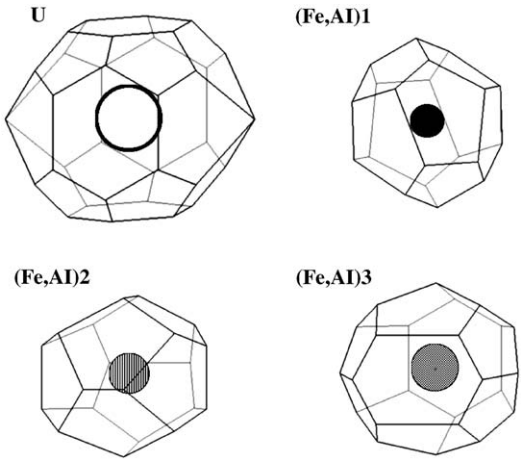

Fig. 2. Wigner–Seitz cells in the UFe_7Al_5 crystal structure.

The Wigner–Seitz cells of the different crystallographic positions in the UFe_7Al_5 compound are shown in Fig. 2. Table 4 summarizes the Wigner–Seitz cell topology and cell volumes of the different UFe_7Al_5 crystallographic sites. As usually observed in the $ThMn_{12}$-type compounds [28], the 8*f* site has the lowest and the 8*i* site the highest Wigner–Seitz cell volumes (Table 4). The calculated volumes for each 8*f*, 8*j* and 8*i* positions are smaller than those estimated for the pure iron and aluminum metals (11.78, 14.19 and 15.39 $Å^3$ for α-Fe, 50%(α-Fe)–50%(Al) and 25%(α-Fe)–75%(Al)), pointing to a higher affinity with the nearest neighbors than in the pure elements, in agreement with the negative solution enthalpies of iron in aluminim and uranium. The large difference between the uranium coordination numbers in UFe_7Al_5 and α-U (20 and 12,

Table 4
Wigner–Seitz cell topology and cell volumes of UFe_7Al_5

Atom	Position	F_3	F_4	F_5	F_6	V_3	V_4	R (Å)	Volume (Å^3)
U	2*a*	0	0	16	4	32	2	1.53	22.44
(Fe,Al)1	8*f*	0	0	12	0	20	0	1.26	11.11
(Fe,Al)2	8*j*	0	0	12	0	20	0	1.35	13.74
(Fe,Al)3	8*i*	0	0	12	2	24	0	1.39	15.07

F_i denotes the number of faces with i vertices and V_j signifies the number of faces per vertex on a Wigner–Seitz cell; R is the weighed radii for each position, considering the atomic occupations.

respectively) does not allow a direct comparison between their Wigner–Seitz cell volumes.

The preferential occupation of the crystallographic positions by iron and aluminum follow the relative order of the Wigner–Seitz cell volumes, with the smallest element (iron) preferring the site with the smallest Wigner–Seitz cell (8*f*) and the largest element (aluminum) the largest site (8*i*). However, the partial iron occupation of the 8*i* site can not be explained only by volumetric constraints and other enthalpic and entropic factors must be considered.

An analysis of the Wigner–Seitz cell volume and shape, and of the related coordination polyhedron, can give extra information on the reliability of the crystallographic fit. The observation of the uranium Wigner–Seitz cell shows the existence of a higher free volume and, consequently, of lower volumetric constraints, along the *c*-axis. This is effectively reflected in the anisotropic temperature factors, with the U_{33} being higher than the other factors. Similar behavior can be observed for 8*j* sites, with the higher temperature factors (U_{11}) being along the direction having the lower spacial constraints (*a*).

The Wigner–Seitz inspection of a certain crystallographic position often offers an alternative procedure for the determination of its coordination number, which is given by the total number of faces of the Wigner–Seitz cell. By using this method, 20, 12, 12 and 14 coordination numbers are obtained for the U (2*a*), (Fe,Al)1 (8*f*), (Fe,Al)2 (8*j*) and (Fe,Al)3 (8*i*) positions of UFe_7Al_5, in total agreement with the previous determination (Table 3).

The above considerations suggest reduced hybridization effects between uranium and most of the other atoms and, consequently, the possibility of an appreciable uranium magnetic moment (the shortest distances between uranium atoms, 4.95 Å, are well above the Hill limit, ~3.4 Å). Strong orbital overlap between (Fe,Al)1 and (Fe,Al)2 and their nearest-neighbor iron and aluminum atoms, and medium overlap between (Fe,Al)3 and the next-nearest neighbors are also expected.

The variation of magnetization with temperature for various magnetic fields is shown in Fig. 3. For fields up to 0.1 T, two magnetic transitions can be observed: a ferromagnetic-type transition, at 363(1) K (T_A), and a less pronounced anomaly, at 275(2) K (T_B), which is smoothed out for higher measurement fields.

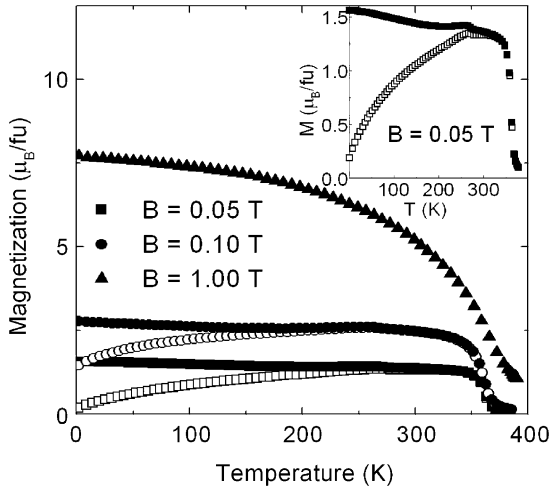

Fig. 3. Temperature dependence of the magnetization for UFe_7Al_5, obtained at different applied fields (squares: 0.5 kOe, circles: 1.0 kOe, up-triangles: 10 kOe; ZFC: open and FC: full symbols). The inset shows in detail the temperature dependence of the magnetization obtained in $B = 500$ Oe.

The dependence of magnetization on the applied field, for values up to 8 T, for various temperatures is shown in Fig. 4. For temperatures below 363 K, the curves are typical of a ferromagnet, the magnetization increasing rapidly at low fields (<0.5 T) and the extrapolated spontaneous magnetization for $T = 0$ K being $m_s = 8.5\,\mu_B$/f.u. For larger applied fields, a linear increase is observed, that can be explained from the polycrystalline character of the samples, with randomly oriented grains.

The magnitude of the T_A transition indicates that it is related to ferromagnetic ordering of the iron atoms as fully confirmed by ^{57}Fe Mössbauer spectroscopy data (see below). The anomaly at 275(2) K can reflect either a rearrangement of magnetic moments or another type of magnetic ordering occurring in the system, such as the ordering of the uranium moments. This anomaly cannot be explained by the existence of small amounts of 66%Fe–34%Al FeAl-type impurities, which have a low-temperature antiferromagnetic transition [29].

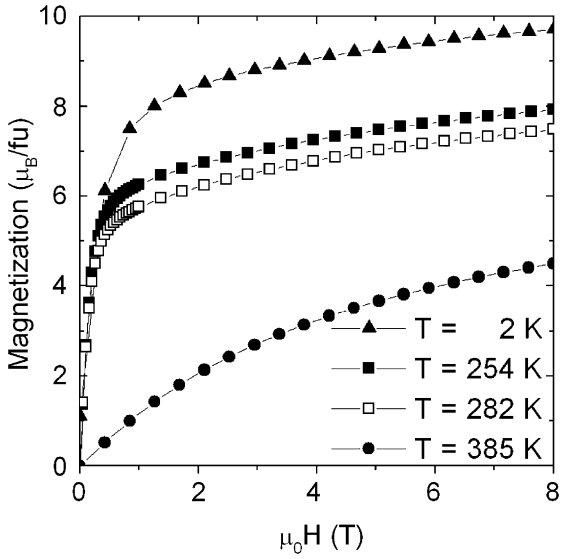

Fig. 4. Magnetization versus magnetic field for UFe_7Al_5 at different temperatures (up-triangle: 2 K, closed square: 254 K, open square: 282 K, closed circle: 385 K).

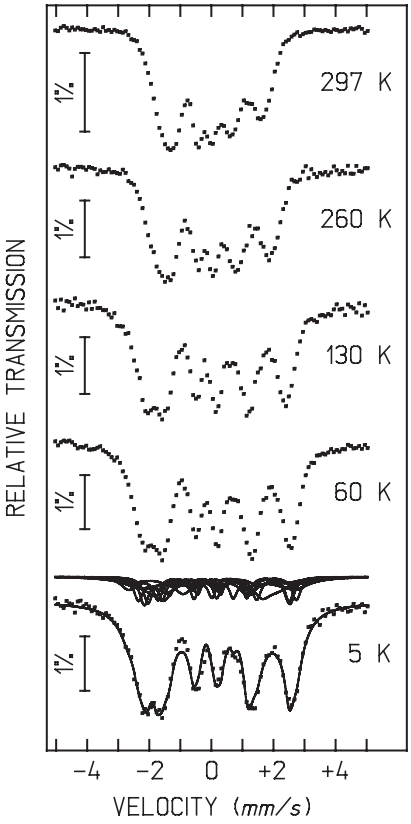

Fig. 5. Mössbauer spectra of UFe_7Al_5 taken at different temperatures. The lines over the experimental points on the spectrum taken at 5 K are the sum of sextets corresponding to Fe atoms on different sites and in different environments. The estimated parameters for these sextets, shown slightly shifted for clarity, are collected in Table 6.

The ^{57}Fe Mössbauer spectra show that in UFe_7Al_5 the iron moments order magnetically above room temperature (Fig. 5). At 5 K, the spectrum is basically similar to that of $UFe_{5.8}Al_{6.2}$ taken at the same temperature [22] although a closer examination reveals that in the UFe_7Al_5 spectrum higher magnetic hyperfine fields are observed.

Mössbauer spectra of the UFe_xAl_{12-x} ($4.2 \leqslant x \leqslant 5.8$) intermetallics below the ordering temperature may only be properly analyzed assuming that the B_{hf} of the iron atoms depend not only on the crystallographic site but also on the number of iron nearest neighbors [22]. The isomer shift, δ, decreases while the magnetic hyperfine field, B_{hf}, increases, as the number of iron nearest neighbors, z, increases.

Assuming the iron and aluminum site distribution deduced from X-ray diffraction data (Table 2) and a statistical occupation of the iron and aluminum atoms on the 8j and 8i sites, the probability of finding m iron atoms in a shell of n nearest-neighbor 8j or 8i sites is given by the binomial distribution function

$$P_n(m) = \frac{n!}{m!(n-m)!} y^m (1-y)^{n-m},$$

where y is the fraction of the 8j or 8i sites occupied by iron atoms. $P_n(m)$ has to be calculated for the 8f (which have $n = 4$ nearest-neighbor 8j sites and $n = 4$ nearest-neighbor 8i sites), for the 8j (which have $n = 2$ nearest-neighbor 8j sites and $n = 4$ nearest-neighbor 8i sites) and for the 8i sites (which have $n = 4$ nearest-neighbor 8j sites and $n = 5$ nearest-neighbor 8i sites). While in the UFe_xAl_{12-x} ($4.2 \leqslant x \leqslant 5.8$) composition range, iron atoms are only located on 8f and 8j sites [22], in UFe_7Al_5 a significant number of iron atoms is present on 8i sites (Table 2). Therefore, for each site $P_n(m)$ has to be calculated twice in order to consider both iron nearest neighbors on 8j and on 8i sites. Knowing the values of all the $P_n(m)$ for each site it is possible to estimate the probability $P(z)$ of finding z nearest-neighbor iron atoms of another iron atom standing on the 8f, on the 8j or on the 8i site. The $P(z)$ values $\geqslant 0.1\%$ are shown in Table 5. From these values, the relative intensities (I) of the corresponding magnetic splittings in the Mössbauer spectra were deduced (Table 5). Due to the large number of different nearest-neighbor configurations with significant probabilities (Table 5) and the strong overlapping of their contributions, the sextets with $I < 6\%$ were not individually considered. Their I was summed to that of the magnetic splitting corresponding to the iron atoms on the same site and with one iron nearest neighbor less or with one more iron nearest neighbor. For this reason, the contribution of all the iron atoms on the 8i site was analyzed by a single sextet and in the whole only eight sextets were considered in the analysis of the spectra.

Depending on the starting values of the refined parameters, several distinct local minima of the

least-squares differences between the calculated functions and the observed spectra are found by the refinement procedure. To each minimum corresponds a different χ^2 and a different final set of refined values for the hyperfine parameters. Starting values have therefore to be carefully chosen. The same criteria used to fit the UFe_xAl_{12-x} with $x \geqslant 4.7$ [22] were applied in the present case: hyperfine parameters of sextets corresponding to iron atoms on the same sites and with the same z were, in first approximation, the same as those estimated for the $x \geqslant 4.7$ spectra; starting values for the B_{hf} and δ of the magnetic splittings attributed to the iron atoms with higher z were chosen assuming that B_{hf} increased and δ decreased as z increased, in agreement with the trend observed in the UFe_xAl_{12-x} ($4 \leqslant x \leqslant 5.8$) case [22].

The total absorption area of the spectra, δ, B_{hf} and the quadrupole shifts, ε for the eight sextets were refined but their I were forced to remain constant and consistent with the above-calculated probabilities $P(z)$.

The final values of the estimated parameters for the 5 K spectrum are shown in Table 6. Among the several analyses of the UFe_7Al_5 spectra with similar final values of χ^2 we believe that the solutions summarized in Table 6 are the closest to real values since (i) the final values of the hyperfine parameters are consistent with those obtained for the UFe_xAl_{12-x} ($4 \leqslant x \leqslant 5.8$) [22]; (ii) they correspond to one of the lowest local χ^2 minima and the agreement between the experimental points on the Mössbauer spectra and the calculated functions is good, as may be seen in Fig. 5.

The Mössbauer data of UFe_7Al_5 is therefore consistent with a similar dependence of δ and B_{hf} on z as found for the UFe_xAl_{12-x} ($4 \leqslant x \leqslant 5.8$). The sextet peaks corresponding to all the iron atoms on the 8*i* sites are broader than the others because the 8*i* sextet is the sextet that represents the largest number of different iron nearest-neighbor arrangements [4] with relative areas larger than 1.4% (Table 4). While δ of iron atoms on 8*i* sites is similar to those of iron atoms on 8*f* and 8*j* sites with z similar to the average z of iron atoms on 8*i* sites, the B_{hf} is significantly higher (Table 6).

This fact may be correlated with the Fe–Fe interatomic distances. As explained in detail in previous reports on the Mössbauer study of UFe_xAl_{12-x} with $4 \leqslant x \leqslant 5.8$ [22] and of other intermetallics with $ThMn_{12}$-type structure, such as $UFe_{10}Si_2$ and $UFe_{10}Mo_2$ [30], an increase in the strength of the Fe–Fe magnetic exchange interactions was always observed when the Fe–Fe interatomic distances increased. The larger B_{hf} for iron atoms on 8*i* sites in UFe_7Al_5 are therefore consistent with the significantly higher average Fe–Fe interatomic distances for the iron atoms on this site (Table 3) and with its higher Wigner–Seitz cell volume (Table 4).

As the temperature increases, all the estimated B_{hf} values decrease and the degree of overlapping of the spectra worsens (Fig. 5). Due to the complexity of the UFe_7Al_5 spectra, no further information is extracted from those obtained above 5 K. Namely, it is not possible to detect any discontinuity in the dependence of B_{hf} on temperature at 275 K. In contrast, in the case of $UFe_{4.2}Al_{7.8}$, whose low-temperature Mössbauer spectra are much simpler than those of UFe_7Al_5 consisting only of three sextets, it is possible to detect a discontinuity in the B_{hf} dependence on temperature, at the temperatures where singularities are observed in the corresponding magnetization curves [13].

Table 5
Probability $P(z)$ of the Fe atoms on the 8*f*, 8*j* and 8*i* sites with z Fe nearest neighbors, in UFe_7Al_5

Site	z		Site	z		Site	z	
8*f*	$\geqslant 8$	0.033	8*j*	$\geqslant 9$	0.011	8*i*	$\geqslant 10$	0.057
	7	0.112		8	0.070		9	0.140
	6	0.244		7	0.225		8	0.257
	5	0.305		6	0.362		7	0.286
	4	0.215		5	0.263		6	0.187
	3	0.080		4	0.069		5	0.066
	2	0.012					4	0.010

Table 6
Estimated parameters from the Mössbauer spectrum of the UFe_7Al_5 sample taken at 5 K

Site	z	I	δ	ε	Γ	B_{hf}	$\langle z \rangle$	$\langle B_{hf} \rangle$
8*i*		11.7	0.09	0.21	0.32	17.0	7.4	17.0
8*j*	$\geqslant 7$	10.0	0.11	0.49	0.25	15.7		
8*j*	6	11.7	0.15	0.40	0.25	14.5	6.0	14.7
8*j*	$\leqslant 5$	10.7	0.21	0.27	0.25	14.0		
8*f*	$\geqslant 7$	8.1	0.09	−0.18	0.25	15.4	5.2	14.2
8*f*	6	13.6	0.14	0.20	0.24	14.4		
8*f*	5	17.0	0.20	0.55	0.25	14.2		
8*f*	$\leqslant 4$	17.1	0.26	−0.43	0.27	13.5		

I, relative areas, are fixed, consistent with the $P(z)$ values in Table 5. δ, isomer shift relative to metallic α-Fe at 295 K; $\varepsilon = (e^2 V_{ZZ} Q/4)(3\cos^2\theta - 1)$, quadrupole shift calculated from $(\phi_1 + \phi_6 - \phi_2 - \phi_5)/2$, where ϕ_n is the shift of the nth line of the magnetic sextet due to quadrupole coupling. Γ, linewidths of the two inner peaks of a sextet; B_{hf}, magnetic hyperfine field. Estimated errors for the sextets with $I > 11\%$ are $\leqslant 0.2$ T for B_{hf}, $\leqslant 0.02$ mm/s for δ, ε, Γ, and for the other sextets $\leqslant 0.4$ T for B_{hf}, $\leqslant 0.03$ mm/s for δ, and $\leqslant 0.04$ mm/s for Γ and ε. $\langle z \rangle$, $\langle B_{hf} \rangle$ are the average z and B_{hf} for each site.

4. Conclusion

The ternary intermetallic compound, UFe_7Al_5, was synthesized and its structure studied by X-ray diffraction. This compound was found to crystallize in the tetragonal $ThMn_{12}$-type structure, belonging to the

series with UFe_xAl_{12-x} general formula. The structure refinement clearly indicates a significant iron concentration in the 8*i* crystallographic position, in contrast with the lower iron compounds of this series ($4 \leqslant x \leqslant 6$) where the 8*i* site is avoided by iron.

The analysis of the nearest-neighbor environments points to a reduced hybridization between uranium and the other atoms (and, consequently, a possibility of an appreciable uranium magnetic moment) and dissimilar orbital overlap between the different iron atoms. The magnetization results indicate the existence of two magnetic anomalies, at 363 and 275 K, the ferromagnetic character strongly increasing below the highest temperature anomaly.

At room temperature, no paramagnetic iron atoms are observed in the Mössbauer spectrum suggesting that the highest temperature anomaly is related to the magnetic ordering of the iron sublattices. The analysis of the 5 K Mössbauer spectrum is consistent with the iron and aluminum site distributions deduced from the analysis of the single-crystal X-ray diffraction data. It further showed a dependence of the isomer shift and magnetic hyperfine fields on the crystallographic site and number of iron nearest neighbors similar to that observed in UFe_xAl_{12-x} ($4 \leqslant x \leqslant 6$) and RFe_xAl_{12-x} ($R = Y$, Lu, $x = 4$, 4.2) compounds [22,31,32]. This analysis brings further evidence for the presence of iron atoms on the 8*i* site. Iron atoms on this site have the largest hyperfine magnetic field values, similar to those reported for iron atoms on the same site for $UFe_{10}Si_2$ [30].

Acknowledgments

This work was partially supported by the exchange Program 2002-ICCTI/CNRS and by FCT (Portugal).

References

[1] H.S. Li, J.M.D. Coey, in: K.H.J. Buschow (Ed.), Handbook of Magnetic Materials, Vol. 1, North-Holland, Amsterdam, 1991, p. 1.
[2] K.H.J. Buschow, in: G.J. Long, F. Grandjean (Eds.), Supermagnets, Hard Magnetic Materials, Kluwer, Dordrecht, 1991, p. 49.
[3] K.H.J. Buschow, A.M. van der Kraan, J. Phys. F 8 (1978) 921.
[4] I. Felner, I. Nowik, J. Phys. Chem. Solids 39 (1978) 951.
[5] A. Baran, W. Suski, T. Mydlarz, J. Less-Common Met. 96 (1984) 269.
[6] A. Baran, W. Suski, T. Mydlarz, Physica B 130 (1985) 219.
[7] P. Schobinger-Papamantellos, K.H.J. Buschow, C. Ritter, J. Alloys Compd. 186 (1998) 21.
[8] G. Bonfait, M. Godinho, P. Estrela, A.P. Gonçalves, M. Almeida, J.C. Spirlet, Phys. Rev. B 53 (1996) R480.
[9] J.A. Paixão, B. Lebech, A.P. Gonçalves, P.J. Brown, G.H. Lander, P. Burlet, A. Delapalme, J.C. Spirlet, Phys. Rev. B 55 (1997) 14370.
[10] K. Recko, M. Biernacka, L. Dobrzynski, K. Perzynska, D. Satula, K. Szymanski, J. Waliszewski, W. Suski, K. Wochowski, G. André, F. Bourée, J. Phys.: Condens. Matter 9 (1997) 9541.
[11] B. Ptasiewicz-Bak, A. Baran, W. Suski, J. Leciejewicz, J. Magn. Magn. Mat. 76–77 (1988) 439.
[12] A.P. Gonçalves, M. Almeida, C.T. Walker, J. Ray, J.C. Spirlet, Mater. Lett. 19 (1994) 13.
[13] M. Kuznietz, A.P. Gonçalves, J.C. Waerenborgh, M. Almeida, C. Cardoso, M. Cruz, M. Godinho, Phys. Rev. B 60 (1999) 9494.
[14] A.P. Gonçalves, H. Noël, in: Proceedings, Actinides 2001, 7P02 Hayama, Japan, November 4–9, 2001.
[15] T.J.B. Holland, S.A.T. Redfern, Mineral. Mag. 61 (1997) 65.
[16] A.C.T. North, D.C. Phillips, F.S. Mathews, Acta Crystallogr. Sect. A 24 (1968) 351.
[17] G. M. Sheldrick, SHELX-97-Program for Crystal Structure Solution and Refinement, University of Göttingen: Göttingen, Germany, 1997.
[18] J.V. Florio, R.E. Rundle, A.I. Snow, Acta Crystallogr. 5 (1952) 449.
[19] T. Hahn (Ed.), International Tables for Crystallography, Space-Group Symmetry, Vol. A, Riedel, Dordrecht, 1983.
[20] E. Koch, W. Fischer, Z. Kristallogr. 211 (1996) 251.
[21] B.J. Gellatly, J.L. Finney, J. Non-Cryst. Solids 50 (1982) 313.
[22] J.C. Waerenborgh, A.P. Gonçalves, M. Almeida Solid State Commun. 110 (1999) 369.
[23] J.D. Hanawalt, Anal. Chem. 10 (1938) 475.
[24] O. Moze, R.M. Ibberson, K.H.J. Buschow, J. Phys. : Condens. Mater. 2 (1990) 1677.
[25] K. Wochowski, P. Burlet, G. André, F. Bourée, W. Suski, J. Phase Equilibria 19 (1998) 423.
[26] P. Estrela, M. Godinho, A.P. Gonçalves, M. Almeida, J.C. Spirlet, J. Alloys Compd. 230 (1995) 35.
[27] B.K. Vainshtein, V.M. Fridkin, V.L. Indenbom, in: M. Cardona, P. Fulde, H.-J. Queisser (Eds.), Modern Crystallography II, Structure of Crystals, Vol. 21, Springer Series in Solid-State Sciences, Springer, Berlin, 1982, p. 71.
[28] M. Melamud, L.H. Bennett, R.E. Watson, J. Appl. Phys. 61 (1987) 4246.
[29] A. Arrot, H. Sato, Phys. Rev. 114 (1959) 1420.
[30] J.C. Waerenborgh, M.S. Rogalski, A.P. Gonçalves, J.B. Sousa, M. Almeida, Solid State Commun. 104 (1997) 271.
[31] J.C. Waerenborgh, P. Salamakha, O. Solugub, A.P. Gonçalves, C. Cardoso, S. Sério, M. Godinho, M. Almeida, Chem. Mater. 12 (2000) 1743.
[32] J.A. Paixão, M. Ramos Silva, J.C. Waerenborgh, A.P. Gonçalves, G.H. Lander, P.J. Brown, M. Godinho, P. Burlet, Phys. Rev. B 63 (2001) 54410.